How and why intralumenal membrane fragments form during vacuolar lysosome fusion

Sevan Mattie[a,†], Erin K. McNally[a], Mahmoud A. Karim[a], Hojatollah Vali[b], and Christopher L. Brett[a,b,*]

[a]Department of Biology, Concordia University, Montréal, QC H4B 1R6, Canada; [b]Department of Anatomy and Cell Biology, McGill University, Montréal, QC H3A 0C7, Canada

ABSTRACT **Lysosomal membrane fusion mediates the last step of the autophagy and endocytosis pathways and supports organelle remodeling and biogenesis. Because fusogenic proteins and lipids concentrate in a ring at the vertex between apposing organelle membranes, the encircled area of membrane can be severed and internalized within the lumen as a fragment upon lipid bilayer fusion. How or why this intralumenal fragment forms during fusion, however, is not entirely clear. To better understand this process, we studied fragment formation during homotypic vacuolar lysosome membrane fusion in *Saccharomyces cerevisiae*. Using cell-free fusion assays and light microscopy, we find that GTPase activation and *trans*-SNARE complex zippering have opposing effects on fragment formation and verify that this affects the morphology of the fusion product and regulates transporter protein degradation. We show that fragment formwation is limited by stalk expansion, a key intermediate of the lipid bilayer fusion reaction. Using electron microscopy, we present images of hemifusion diaphragms that form as stalks expand and propose a model describing how the fusion machinery regulates fragment formation during lysosome fusion to control morphology and protein lifetimes.**

Monitoring Editor
Suresh Subramani
University of California, San Diego

Received: Nov 12, 2015
Revised: Nov 4, 2016
Accepted: Nov 18, 2016

INTRODUCTION

All eukaryotic cells must recycle biomaterials. Lysosomes are single lipid bilayer–encased organelles containing hydrolases that perform this important function (de Duve and Wattiaux, 1966). To be recycled, biomaterials within the cell (through the autophagy pathway) or outside the cell (by endocytosis or phagocytosis) are first encapsulated by membranes. Newly formed compartments undergo heterotypic membrane fusion with lysosomes to expose their contents to lumenal hydrolases, permitting breakdown of macromolecules into their constituents, which are exported to the cytoplasm by lysosomal transporters for reuse (Pisoni and Thoene, 1991; Luzio *et al.*, 2007). Sometimes lysosomes must be remodeled to accommodate this function. For example, lysosomes undergo homotypic fusion to form tubular networks within immune cells upon activation, presumably to aid in processing antigens (Knapp and Swanson, 1990; Mrakovic *et al.*, 2012). Thus both homotypic and heterotypic membrane fusion events are critical for lysosome function.

A working model of the lysosome membrane fusion process has been developed primarily based on studying vacuolar lysosomes within *Saccharomyces cerevisiae* (baker's yeast; Wickner, 2010). This process requires evolutionarily conserved machinery that orchestrates at least four distinct stages: priming, tethering, docking, and fusion. In brief, priming involves unraveling *cis*–soluble *N*-ethylmaleimide–sensitive factor attachment protein receptor (SNARE) complexes to accommodate the next round of membrane fusion. Tethering is operationally defined as occurring when apposing vacuole membranes make first contact and requires activation of the

This article was published online ahead of print in MBoC in Press (http://www.molbiolcell.org/cgi/doi/10.1091/mbc.E15-11-0759) on November 23, 2016.

C.L.B. and H.V. conceived the project. S.M. and H.V. optimized methods for imaging vacuoles by electron microscopy. S.M. and C.L.B. prepared the vacuole fusion reactions for imaging. S.M. performed all electron microscopy. M.A.K. performed lipid and content mixing experiments. E.K.M. performed HILO imaging. S.M. and E.K.M. conducted quantitative analyses of micrographic data. C.L.B. wrote the manuscript.

[†]Present address: Montreal Neurological Hospital and Institute, McGill University, Montréal, QC H3A 2B4, Canada.

*Address correspondence to: Christopher L. Brett (christopher.brett@concordia.ca).

Abbreviations used: ALPS, amphipathic lipid-packing sensor; GFP, green fluorescent protein; HILO, highly inclined and laminated optical sheet; HOPS, homotypic fusion and protein sorting; SNARE, soluble *N*-ethylmaleimide–sensitive factor attachment protein receptor; TEM, transmission electron microscopy; TIRF, total internal reflection fluorescence.

Rab-GTPase Ypt7 and subsequent recruitment of the multisubunit tethering homotypic fusion and protein sorting complex (HOPS). Docking occurs when fusogenic lipids and proteins accumulate at the vertex ring formed between organelles, the future site of lipid bilayer fusion (Wang *et al.*, 2003). At this stage, HOPS facilitates the initial assembly of *trans*-SNARE complexes composed of one arginyl (R)-SNARE (Nyv1) and three glutaminyl (Q)-SNAREs (Vti1, Vam3, and Vam7) that span apposing membranes (Starai *et al.*, 2008). Membrane fusion is the final step by which partially assembled *trans*-SNARE complexes completely zipper to drive lipid bilayers together, completing the reaction (Schwartz and Merz, 2009). Of importance, bilayer fusion occurs along the vertex ring, excising the encircled area of membrane called the boundary to form an intralumenal fragment that is degraded by lumenal hydrolases (Wang *et al.*, 2002). This is a unique feature of organelle membrane fusion, as compared with vesicle fusion, which is believed to mediate degradation of resident integral membrane proteins (Wang *et al.*, 2002) and regulate organelle morphology by effectively changing the membrane surface area of the product (Brett and Merz, 2008; Chan and Marshall, 2010). Although it is clear that formation of this fragment likely plays an important role in lysosome biology, many outstanding questions remain: Must a fragment form to accommodate bilayer fusion? What mechanisms drive this process? How is the fragment actually formed?

Little is known about how these fragments form, but it must occur during the last stage of the process when apposing lipid bilayers merge. Wickner and colleagues proposed hypothetical models describing this process (Wang *et al.*, 2002; Jun and Wickner, 2007), on the basis of evidence from studies using synthetic systems and computational modeling to describe fusion of small vesicle membranes (Diao *et al.*, 2012, 2015; Hernandez *et al.*, 2012; Warner and O'Shaughnessy, 2012; Risselada *et al.*, 2014). Initially, the outer leaflets of apposing lipid bilayers mix, forming a lipid stalk that bridges the membranes (Figure 1A). On expansion of the stalk within the vertex ring, the intact inner leaflets make contact, forming a hybrid bilayer called a hemifusion diaphragm that separates the lumenal contents of the two organelles (Chernomordik and Kozlov, 2008; Harrison, 2008). Next a pore is formed within this diaphragm that rapidly expands, allowing lumenal contents to mix and the two membranes to completely merge. Because the fusion machinery is arranged in a ring, it is hypothesized that this reaction will sever the bilayers through lateral propagation of the pore along the vertex, entrapping the encircled membrane, which becomes an intralumenal fragment (Wang *et al.*, 2002, 2003). However, this outcome relies on the assumption that the transition between stalk and pore formation occurs rapidly because if there is a delay in pore formation after a stalk has formed, then this model predicts that the stalk may have sufficient time to expand, creating a hemifusion diaphragm that occupies the entire area within the vertex ring. When a pore forms, it will dilate across the entire disk-shaped contact site, no membrane will be entrapped, and no fragment will form. The contribution of the fusion machinery to each intermediate is not clear; however, it

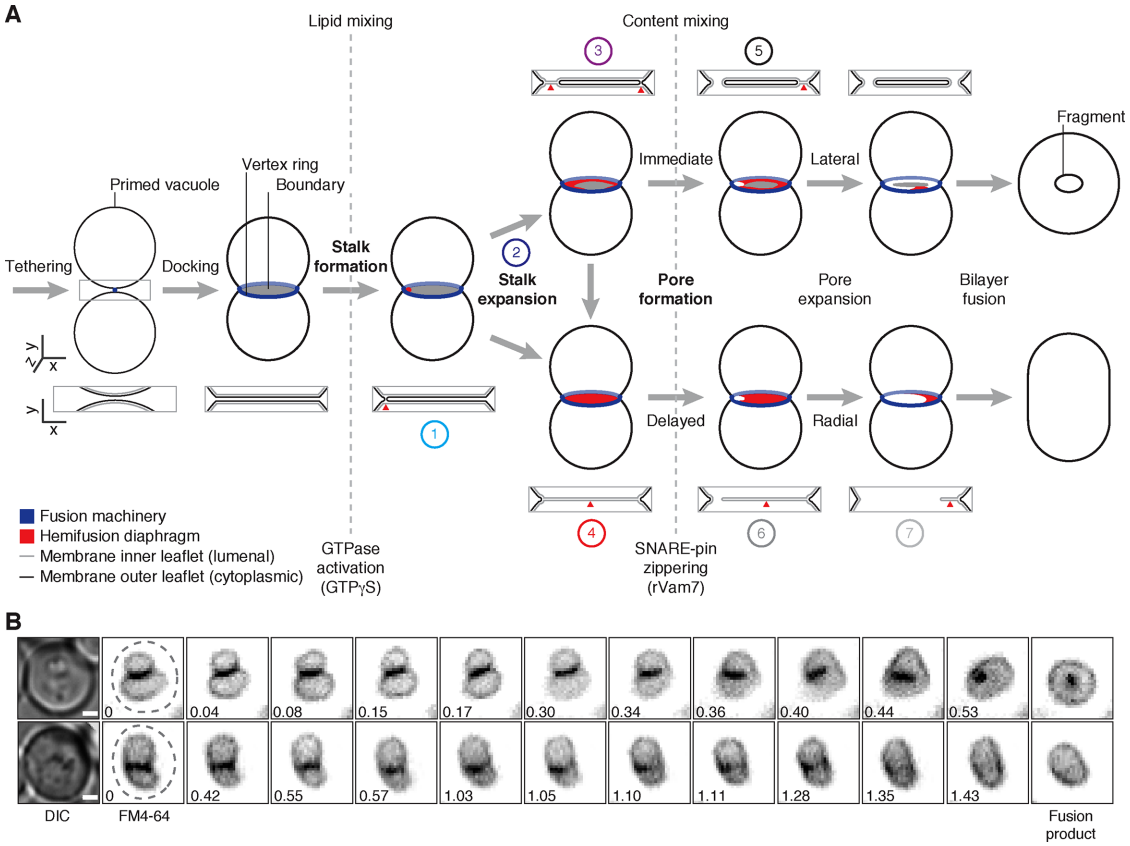

FIGURE 1: Fragment formation during vacuolar lysosome fusion. (A) Working model describing how intralumenal membrane fragments form during homotypic vacuolar lysosome membrane fusion. Numbers indicate reaction intermediates that were visualized using TEM and are shown in Figure 5D. (B) Live yeast cells stained with FM4-64 to label vacuole membranes were imaged using HILO microscopy. Examples of vacuole fusion events are shown as a series of inverted micrographic images acquired over time (minutes). Dashed lines outline each cell observed by differential interference contrast. Scale bars, 1 μm.

was proposed that SNARE zippering is critical for pore formation (Reese and Mayer, 2005); thus components that function earlier in the pathway (e.g., Ypt7 and HOPS) are believed to orchestrate upstream events, that is, stalk formation. For example, constitutive activation of small GTPases like Ypt7 with GTPγS causes accumulation of hemifusion intermediates and thus is believed to promote all events preceding pore formation (Reese *et al.*, 2005; Jun and Wickner, 2007). However, these hemifusion intermediates have not been visualized during native organelle membrane fusion, nor has the organelle lipid bilayer fusion reaction been studied in detail. Thus, to determine how fragments may form during vacuolar lysosome fusion, we used cell-free assays, as well as light and electron microscopy, to test this model and better understand why fragments form during organelle fusion.

RESULTS

Fragment formation is regulated during vacuolar lysosome fusion

To better understand how fragments are formed, we first asked whether fragments are needed to complete vacuole fusion. If so, then all vacuole fusion events should produce a fragment. To test this hypothesis, we imaged vacuole fusion events with yeast live cells stained with FM4-64, a fluorescent dye that selectively stains vacuole membranes. Within an actively growing yeast culture, we find that most fusion events create a spherical organelle containing an internal fragment (Figure 1B; Supplemental Video S1). However, 6.1% of all fusion events observed ($n = 164$) do not produce visible membrane fragments and generated a single, capsule-shaped organelle (Figure 1B; Supplemental Video S2). This finding helps illustrate the effect of fragment formation on vacuole morphology. Of greater importance, however, it reveals that fragment formation is not required for vacuole membrane fusion in living cells and thus suggests that we could study the underlying mechanism(s) by identifying conditions that favor or prevent fragment formation.

Fusion machinery controls rates of stalk and pore formation to regulate fragment formation and organelle morphology

What mechanisms drive fragment formation? According to our working model (Figure 1A), mechanisms that alter the extent of stalk expansion during the lipid bilayer fusion reaction should affect fragment formation. Based on previous reports, treating isolated vacuoles with the nonhydrolyzable GTP analogue GTPγS causes the extent of lipid mixing (a measure of stalk formation) to exceed content mixing (a measure of pore formation), suggesting the accumulation of stable hemifusion diaphragms (Reese *et al.*, 2005; Jun and Wickner, 2007). We replicated these results (Figure 2, A–C) and found that 0.2 mM GTPγS stimulated the rate of lipid but not content mixing (Figure 2D), thus extending the delay between stalk and pore formation when the stalk is predicted to expand. GTPγS constitutively activates small GTPases, including Ypt7, the vacuolar Rab-GTPase that orchestrates membrane tethering and docking before SNARE-pin zippering required for pore formation, the rate-limiting step of the reaction (Eitzen *et al.*, 2000; Reese and Mayer, 2005). Thus we reasoned that directly stimulating SNARE zippering with the recombinant Q-SNARE protein Vam7 (rVam7), which bypasses the need for Ypt7 activation, should have the opposite effect on the delay between stalk and pore formation compared with GTPγS (Thorngren *et al.*, 2004; Schwartz and Merz, 2009). Addition of 100 nM rVam7 increased lipid and content mixing to the same extent, suggesting that hemifusion intermediates did not accumulate (Figure 2, A–C), and, as anticipated, rVam7 reduced the delay between stalk and pore formation (Figure 2D). Pretreating vacuoles with GTPγS to activate Ypt7 (preventing bypass) before stimulating fusion with rVam7 reduced the effect of rVam7 on lipid and content mixing (Figure 2, A–C), and although onset of stalk and pore formation was quicker, the delay between these events was similar to control conditions (Figure 2D). These results are consistent with previous work suggesting that active Ypt7 recruits HOPS to assemble and proofread *trans*-SNARE complexes before zippering (Starai *et al.*, 2008; Zick and Wickner, 2013), by which activating Ypt7 with GTPγS before addition of rVam7 enforces SNARE proofreading and thus extends the time required for pore formation to occur.

Having identified conditions that change the time permitted for stalk expansion during the lipid bilayer fusion reaction, we sought to examine their effects on fragment formation. Visual examination of the fusion products confirmed our prediction (Figure 2E), by which GTPγS prevented and rVam7 promoted formation of fragments as compared with control conditions. These data were compared with the time interval between stalk and pore formation calculated for each condition (Figure 2G), revealing a strong negative correlation ($r^2 = 0.96$) between stalk expansion and fragment formation, validating our model. It is also possible that a change in the size of the area within the vertex ring called the boundary could contribute to our observations—for example, GTPγS may cause the boundary to shrink to a small point, which would prevent formation of visible fragments upon fusion. To eliminate this possibility, we measured the length of the boundary during fusion (Figure 2H) and found that addition of GTPγS, rVam7, or both had no significant effects on boundary size as compared with control conditions and thus showed no relationship with fragment formation. To confirm that the observed effects on intralumenal fragment formation alter morphology of the fusion product, we measured the change in organelle surface area before and after fusion and normalized it to content mixing data to estimate the change in surface area relative to the extent of vacuole fusion under each condition (Figure 2I). Fusion products have significantly larger surface areas in the presence of GTPγS compared with control, when fewer fragments are formed during fusion (Figure 2J). Adding rVam7 to fusion reactions reduced surface area compared with control conditions, when the most fragments were observed. Although it is not clear why adding GTPγS and rVam7 causes a decrease in surface area compared with control, this result demonstrates that addition of rVam7 counters the effect of GTPγS on fusion. All things considered, our findings suggest that changing the activities of the fusion machinery affects the time interval between stalk and pore formation to determine the extent of fragment formation, which, in turn, affects the morphology of the fusion product.

Stalk expansion prevents formation of membrane fragments and transporter protein degradation

Because stalk expansion is central to our model of fragment formation, we sought to visualize the resulting hemifusion diaphragms that should occur during the vacuolar lysosome fusion reaction. On the basis of an approach originally applied by Rudolf Volkmer, Andreas Herrmann, and colleagues to study these intermediates using synthetic giant unilamellar proteoliposomes (Nikolaus *et al.*, 2010), we monitored the membrane distribution of green fluorescent protein (GFP)–tagged polytopic proteins during homotypic vacuole fusion in vitro using fluorescence microscopy. We reasoned that if a hemifusion diaphragm exists at the interface between organelles, then these transmembrane domain–containing proteins should be excluded because biophysical constraints prevent them from entering a hybrid bilayer composed of lumenal-facing leaflets on both sides, that is, the hydrophobic, cytoplasmic face of the polytopic

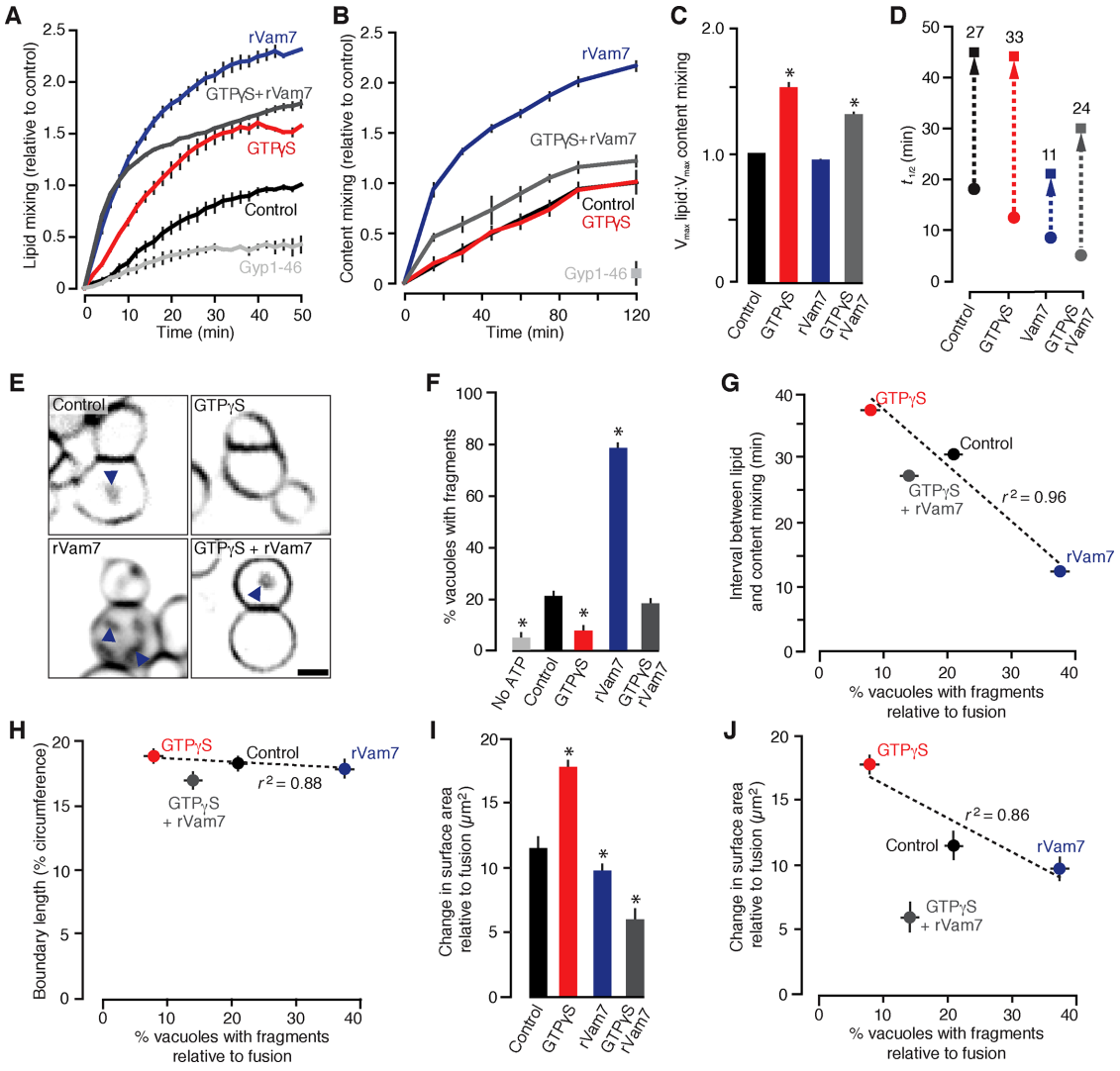

FIGURE 2: GTPγS and rVam7 have opposing effects on the time interval between stalk and pore formation, fragment formation, and surface area during vacuole fusion. Lipid mixing (A) or content mixing (B) was recorded during in vitro homotypic vacuole fusion reactions in the absence (control) or presence of 100 nM rVam7, 0.2 mM GTPγS, or both ($n \geq 6$). As negative control, 3.2 μM Gyp1-46, a Rab-GTPase inhibitor, was added to reactions to prevent fusion. (C) Maximum lipid mixing and content mixing values observed as ratios for each condition. (D) Times at half-maximal lipid mixing (circles) and content mixing (squares); time intervals between events were calculated (numbers) and are shown (arrow). (E) Images of FM4-64 stained vacuoles obtained 60 min after fusion was initiated. Arrowheads indicate intralumenal fragments. Scale bar, 2 μm. Using micrographs of fusion reactions, we calculated the percentage of vacuoles with intralumenal membrane fragments (F) and compared these values to time intervals between stalk and pore formation (G), boundary length (H), or the change in surface area relative to number of fusion events (as assessed by content mixing; I, J) for each condition ($n = 324$–802). Asterisks indicate data points significantly different from control ($p < 0.05$).

protein cannot cross the bilayer to enter the diaphragm (Figure 3A; Nikolaus *et al.*, 2010). We chose to study Vph1, the stalk subunit of the V-type H^+-ATPase, because it is composed of seven transmembrane segments and a bulky cytoplasmic domain (Forgac, 2007; Tokunaga *et al.*, 2008) and is uniformly distributed on vacuole membranes during fusion under standard conditions (Wang *et al.*, 2002). However, Vph1 may play a role in the fusion reaction (Bayer *et al.*, 2003), which could interfere with the interpretation of our results. Although other proteins were also reported to have similar a distribution on vacuole membranes (Vac8, Pho8; Wang *et al.*, 2002), they lack transmembrane domains, do not possess bulky cytoplasmic domains, are also found in the lumen, or are also implicated in the fusion reaction (e.g., Veit *et al.*, 2001). Thus we chose to also study Cot1, a metal transporter predicted to contain six transmembrane domains that is uniformly distributed on vacuole membranes but not implicated in the fusion reaction (Conklin *et al.*, 1992).

Under control conditions, Vph1-GFP and Cot1-GFP are uniformly distributed on vacuole membranes stained with FM4-64, are present at vacuole contact sites, and are internalized upon vacuole bilayer fusion (Figure 3, B and C; Wang *et al.*, 2002), although we observed a few contact sites (<1%) that lacked GFP (Figure 3D). When 0.2 mM GTPγS was added to vacuole fusion reactions, Vph1-GFP and Cot1-GFP were excluded from many contact sites (>15%; Figure 3, B–D) suggesting the presence of hemifusion diaphragms that span the entire area within the vertex ring. In contrast, Vph1-GFP and Cot1-GFP were present at all contact sites and on usually

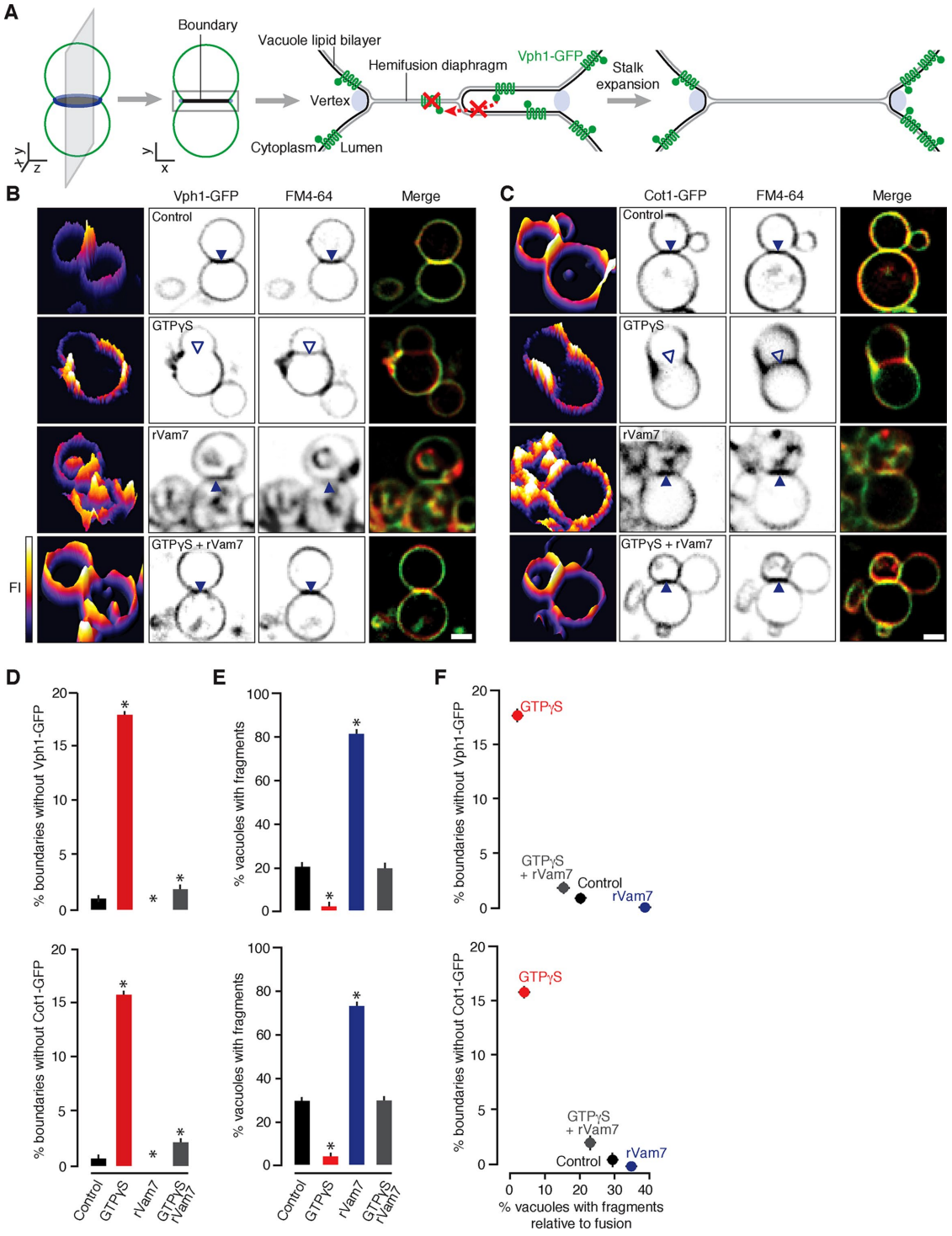

FIGURE 3: Hemifusion diaphragm expansion inversely correlates with fragment formation. (A) Reasoning behind the assay used to detect hemifusion diaphragms by HILO microscopy during homotypic vacuole fusion. Fluorescence micrographs of vacuoles isolated from yeast expressing Vph1-GFP (B) or Cot1-GFP (C) and stained with FM4-64 acquired 30 min after fusion were initiated in the presence of 0.2 mM GTPγS, 100 nM rVam7, or both. Interfaces containing (closed arrowheads) or lacking (open arrowheads) GFP fluorescence are indicated. Left, GFP fluorescence intensity profile plots. Scale bars, 1 μm. The percentage of vacuole contact sites that do not contain Vph1-GFP or Cot1-GFP (D) was calculated and compared with the percentage of vacuoles with internal fragments (E, F; $n \geq 132$). Asterisks indicate data points significantly different from control ($p < 0.05$).

large internal membrane fragments that accumulated within the lumen of fusion products in the presence of 100 nM rVam7. Consistent with data shown in Figure 2, F and J, we observed significantly fewer fragments in the presence of GTPγS and more when rVam7 is present compared with control conditions (Figure 3E), representing a negative relationship between fragment formation and the

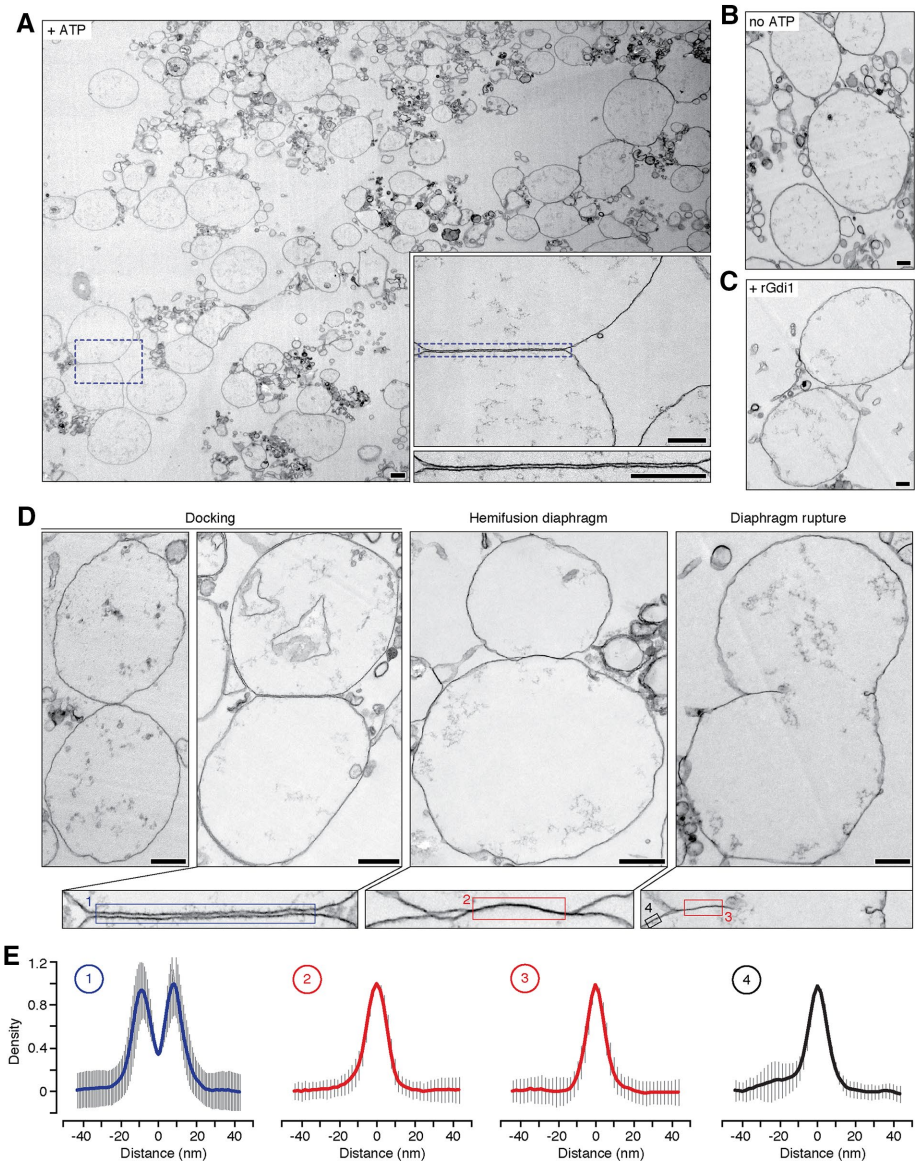

FIGURE 4: Vacuole membrane docking and hemifusion visualized by transmission electron microscopy. (A) Transmission electron micrograph of a vacuole fusion reaction under control conditions (+ATP) at 30 min. Boxes are higher-magnification images illustrating a docking site between apposing organelles. Scale bars, 200 nm. Images of vacuoles incubated without ATP (B) or with ATP and recombinant Gdi1 protein, a Rab-GTPase inhibitor (14 μm; C) are shown as negative controls. Scale bars, 200 nm. (D) Top, transmission electron micrographs of docked vacuole membranes, a hemifusion diaphragm, and ruptured diaphragm. Bottom, higher-magnification images of membrane interfaces. Scale bars, 500 nm. (E) Averages of linear density plots within the areas shown in D (n = 10–88; error bars represent SD). Scale bars, 50 nm.

absence of GFP from contact sites where hemifusion diaphragms are likely present (Figure 3F). When rVam7 was added to vacuoles pretreated with GTPγS, Vph1-GFP and Cot1-GFP were observed at contact sites, which coincided with the reappearance of intralumenal fragments (Figure 3, B–F). In all, these findings suggest that the fusion machinery regulates hemifusion diaphragm expansion at contact sites between organelles, and this prevents formation of intralumenal fragments during fusion.

Hemifusion diaphragms observed by electron microscopy

Next we used transmission electron microscopy (TEM) to visualize the intermediates important for fragment formation during vacuolar lysosome fusion reaction in vitro (Figure 4A). Under control conditions, 17.9% of the vacuoles observed contacted an adjacent vacuole and formed a flat, extended interface where apposing membranes were often uniformly separated by 8.14 ± 0.09 nm (n = 518). These images are suggestive of vacuole docking, when the fusion machinery accumulates at the vertex ring immediately before bilayer fusion (Wang *et al.*, 2002, 2003). These interfaces were not observed in the absence of ATP (Figure 4B) or in the presence of recombinant Gdi1 protein, a Rab-GTPase inhibitor (Figure 4C), when the fusion reaction was blocked, confirming that the observed structures are intermediates of the vacuole bilayer fusion reaction. Closer examination of these interfaces revealed some contact sites where no intermembrane space was detected at the interface (Figure 4D). Although individual leaflets of the bilayers were not resolved, the membrane thickness in this area was similar to the thickness of a single lipid bilayer (Figure 4E). Thus we suspect that these structures are hemifusion diaphragms formed during organelle membrane fusion. We also observed ruptured hemifusion diaphragms indicative of pore formation and expansion (Warner and O'Shaughnessy, 2012).

We validated our findings by examining vacuolar lysosome fusion reactions that were 1) stained with osmium, Epon-embedded, cut into thick sections, and imaged using electron tomography or 2) flash frozen without staining or embedding and imaged using cryo-EM. Tomography reveals extended hemifusion diaphragms deep within the sample, confirming that sectioning is not causing membrane collapse that could be observed as hemifusion at the surface (Figure 5A and Supplemental Videos S3 and S4). Images of cryogenically prepared samples also validate our observations made by TEM (Figure 5B): docked vacuoles show long, flat interfaces in which apposing membranes are separated uniformly by 8.02 ± 0.18 nm (n = 35), and structures suggestive of extended hemifusion diaphragms were observed. Thus we are confident that the embedding and sectioning methods used for TEM are not altering native vacuole morphology. Although further analysis by cryo-EM would be optimal, imaging proved to be technically challenging due to excessive sample thickness (vacuole diameter is 2 μm on average), which limited electron transmission. Hence we resorted to standard TEM for the remainder of our studies, as initial observations were similar using both methods.

Fusion reaction intermediates visualized by EM validate the model of fragment formation

Under standard reaction conditions, we observed only a single reaction intermediate before rupture: a metastable hemifusion

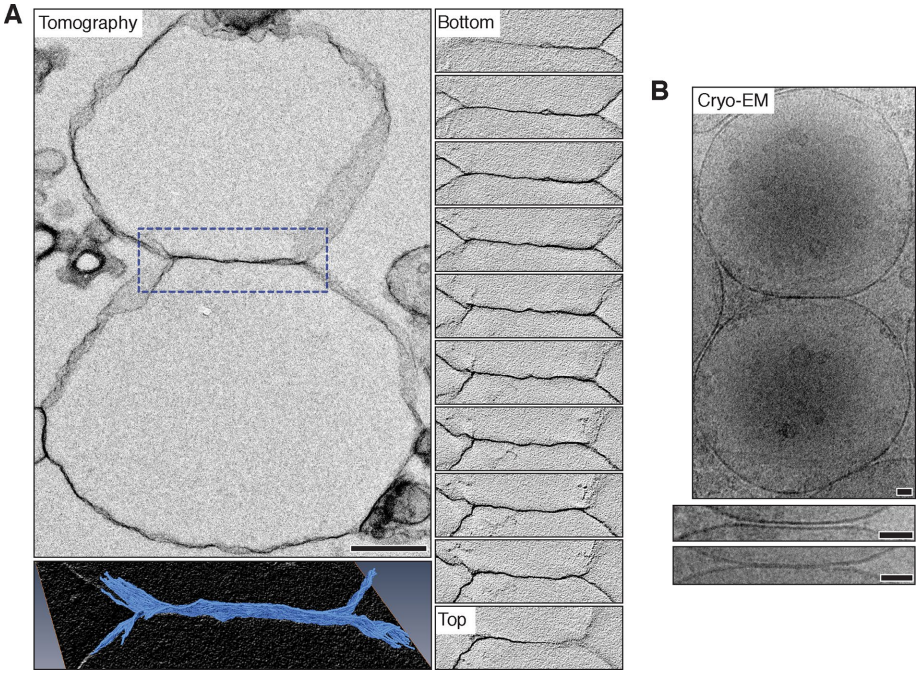

FIGURE 5: Vacuole membrane hemifusion confirmed by electron tomography and cryo–electron microscopy. (A) Top left, vacuole hemifusion diaphragm obtained using electron tomography. Serial sections of the boxed area containing the interface are shown (right; Supplemental Video S3). Scale bar, 500 nm. Bottom left, three-dimensional reconstruction of the interface at higher magnification. Supplemental Video S4 illustrates the reconstruction. (B) Top, cryo–electron micrograph of an in vitro vacuole fusion reaction. Examples of docked vacuole membranes (middle) and a hemifusion diaphragm (bottom) are shown at high magnification. Scale bars, 50 nm.

diaphragm. This is not surprising, given that bilayer fusion proceeds rapidly after docking (Warner and O'Shaughnessy, 2012) and pore formation is rate limiting (Reese and Mayer, 2005; Floyd *et al.*, 2008; Pieren *et al.*, 2010). However, these observations are not sufficient to understand the bilayer fusion reaction in detail. Thus, to increase frequency and diversity of intermediates, we added 0.2 mM GTPγS to fusion reactions and visualized them at 30 min into the fusion reaction, when hemifusion intermediates should be most abundant. As expected, hemifusion diaphragms accumulated in the presence of GTPγS but not in the presence of rVam7 (Figure 6, A and B), consistent with observations made when fusion reactions were not subjected to fixation (Figures 2 and 3). Under all conditions, apposed membranes were uniformly separated by ~8 nm when docked (as when imaged by cryo-EM; Figure 6C). This distance accommodates partially zippered *trans*-SNARE complexes (Li *et al.*, 2007) known to assemble at this stage of the fusion reaction before bilayer fusion (Starai *et al.*, 2008; Schwartz and Merz, 2009). Thus our findings suggest that docked membranes are juxtaposed to accommodate *trans*-SNARE complex formation and bilayer merger across the entire interface.

Closer examination of the vacuole membrane interfaces observed in the presence of GTPγS revealed diverse morphologies (Figure 6D) that we arranged to describe the possible sequential order of intermediates responsible for vacuole bilayer fusion (Figure 1A). These images provide critical visual evidence to support our working model of lysosomal vacuole membrane fusion, in which two fusion products may arise, depending on the pathway of hemifusion intermediates selected: Initially a stalk forms and expands near the vertex ring where fusogenic lipids and proteins are concentrated (Figure 6D, Example 1). This stalk can further expand toward the center of the contact site (Example 2), laterally along the vertex ring (Example 3), or possibly radially to span the entire area within the vertex ring (Example 4). If a pore forms before the hemifusion diaphragm spans the entire interface (Example 5), then membrane can be entrapped and internalized as the pore expands through the diaphragm. However, if the hemifusion diaphragm is permitted to extend across the entire interface, then subsequent pore formation (Example 6) and expansion (Example 7) will result in a fusion product without an internalized membrane fragment. Although we present two intermediate pathways, we recognize that the proposed mechanisms of stalk expansion may not be mutually exclusive. Furthermore, these data do not exclude the possibility that stalks or pores may form at multiple sites along the vertex ring as previously proposed (Wang *et al.*, 2002). However, we argue that regardless of these possible topological variations, all of the data presented suggest that the size of the hemifusion diaphragm formed during the bilayer fusion reaction inversely correlates with the amount of membrane internalized.

DISCUSSION

Vacuolar lysosome fusion through hemifusion

Here we provide empirical evidence that support a model of lysosome membrane fusion through hemifusion (Figure 1A): 1) Using fluorescence microscopy to record individual vacuolar lysosome fusion events in living cells, we show that a small fraction of fusion events do not produce an intralumenal fragment, a predicted outcome that requires hemifusion (Figure 1B). 2) Using lipid (R18-dequenching) and content mixing (lumenal β-lactamase complementation) assays, we confirmed that the extent of lipid mixing exceeded content mixing in the presence of GTPγS (Figure 2, A–C; Jun and Wickner, 2007). We used these data to estimate time constants for stalk and pore formation and found that the time between these events—when hemifusion diaphragms form—is extended in the presence of GTPγS (Figure 2D). 3) By tracking the membrane distribution of GFP-tagged polytopic proteins (Vph1, Cot1) during fusion using fluorescence microscopy, we observe the exclusion of these probes from boundary membranes, indicative of the presence of a stable hemifusion diaphragm in the presence of GTPγS (Figure 3). By studying fixed samples of isolated vacuoles undergoing fusion in vitro using TEM, electron tomography, and cryo-EM, we present micrographs showing membrane structures at organelle interfaces that resemble hemifusion intermediates (Figures 4–6). This data set also supports our model of intralumenal fragment formation during organelle fusion (Figure 1A) in which an inverse correlation between the appearance of extended hemifusion diaphragms and intralumenal fragments was observed using multiple approaches.

In all, these results support the idea that hemifusion to fusion is a universal mechanism for biological membrane fusion. Our findings are comparable to those observed in studies of viral membrane fusion or synaptic vesicle fusion, as well as using reconstituted systems and computational molecular dynamics simulations (Chernomordik and Kozlov, 2008; Harrison, 2008; Hernandez *et al.*, 2012; Warner and O'Shaughnessy, 2012; Risselada *et al.*, 2014),

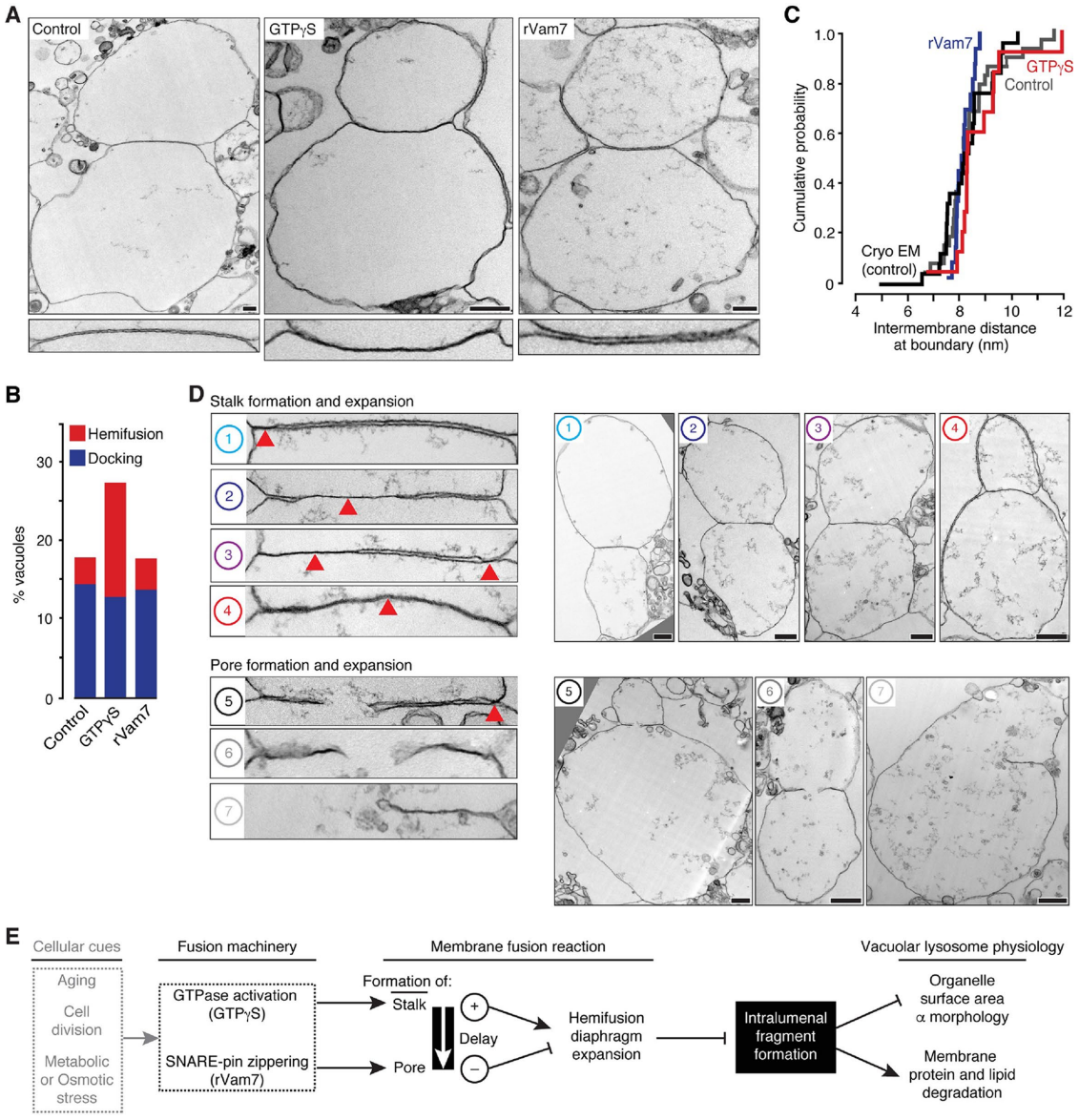

FIGURE 6: Characterization of hemifusion intermediates that underlie fragment formation and their potential contribution to cellular physiology. (A) Top, transmission electron micrographs of vacuole fusion reactions in the absence and presence of 0.2 mM GTPγS obtained at 30 min or 100 nM rVam7 at 10 min. Bottom, interfaces at higher magnification. Scale bars, 250 nm. Electron micrographs were used to calculate (B) percentages of vacuoles engaged in docking or hemifusion ($n \geq 200$) or (C) intermembrane distances at docked interfaces ($n \geq 13$). (D) Transmission electron micrographs showing examples of different hemifusion intermediates observed in vacuole fusion reactions containing 0.2 mM GTPγS. Left, higher-resolution images of interfaces between adjacent vacuoles shown on the right. Numbers correspond to intermediates of the vacuole membrane fusion reaction illustrated in Figure 1A. Red arrowheads indicate hemifusion diaphragms. Scale bars, 500 nm. (E) Model describing how intralumenal fragment formation is regulated and may contribute to changes in lysosomal vacuole physiology in response to cellular cues.

including recent reports of hemifusion diaphragms visualized during SNARE-mediated fusion of proteoliposomes by cryo-EM (Diao *et al.*, 2012, 2015; Hernandez *et al.*, 2012). During synaptic vesicle fusion, hemifusion may be important for fast pore opening or kiss-and-run fusion events underlying synaptic transmission. However, during lysosome fusion, hemifusion controls the extent of membrane internalization, suggesting an alternative physiological purpose. Fragment formation is a unique feature of organelle fusion that requires the fusion machinery to organize into a ring with a large diameter (up to 2 μm; Figure 6D) instead of at a point on a small vesicle (~0.1 μm in diameter). This distinction gives rise to two important questions: How are large hemifusion diaphragms stabilized? Where does stalk and pore formation occur?

Models of protein-free lipid bilayer fusion suggest that hemifusion diaphragms are transient and unstable and must be small to support membrane fusion. Furthermore, the surface area of the inner leaflet must become much greater than that of the outer leaflet to support stalk expansion over large areas, making them unlikely to occur (Chernomordik and Kozlov, 2008). However, extended hemifusion diaphragms similar to those presented here

(Figures 4–6) have been observed during fusion of synthetic giant unilamellar liposomes (Nikolaus *et al.*, 2010), suggesting that large hemifusion diaphragms can be stabilized. Although the basis of this is not understood, we speculate that three mechanisms may contribute to these observed structures during lysosome fusion: lysosomal lipid transporters implicated in vacuole fusion could rapidly translocate phospholipids within membranes to adjust the surface areas of the inner and outer leaflets (e.g., Neo1; Wu *et al.*, 2016), fusogenic proteins that tether membranes at the vertex ring encircling this intermediate structure may act to both limit expansion and stabilize it (Hickey and Wickner, 2010), or lipids within the lumen could serve as a reserve to feed the inner leaflet to increase its surface area, perhaps through the activity of Ncr1 (Berger *et al.*, 2005; Li *et al.*, 2015b), as osmium-stained lipids are frequently observed within the vacuole lumen within close proximity of the inner leaflet of the membrane (e.g., Figure 6D).

Ypt7, HOPS, and SNAREs, as well as other fusogenic proteins and lipids, concentrate at the vertex ring (Wang *et al.*, 2003; Fratti *et al.*, 2004), the site of highest membrane curvature (as observed by light and electron microscopy; Figures 3 and 6). Thus it has been proposed that stalk and pore formation should originate from this site (Wang *et al.*, 2002; Jun and Wickner, 2007). Although our study offers insight into how the subreactions of bilayer fusion may be temporally regulated to determine outcome, we were unable to spatially map sites of stalk and pore formation. This is because contact areas between vacuolar lysosomes are too large to completely image in three dimensions using methods used in our study. Instead, we were able to visualize only narrow portions of each contact site. Thus it is possible that sites of stalk and pore formation may have originated out of the plane of view and extended into the field that was visualized. To overcome this issue, we plan to image entire contact sites using new state-of-the-art methods in volumetric EM (e.g., automated focused-ion-beam scanning EM), which will provide a more comprehensive understanding of this process. Mapping these sites will also help us understand how this process may differ from SNARE-independent mitochondrial outer membrane fusion, where the fusion machinery arranges into a ring between apposing membranes as well but pore formation and expansion occur at a single site, preventing formation of a membrane fragment within the intermembrane space (Brandt *et al.*, 2016).

GTPases and SNAREs regulate fusion subreactions to control intralumenal fragment formation

We also provide data that offer mechanistic insight into how the fusion machinery may contribute to subreactions of organelle lipid bilayer fusion. This machinery determines the length of the time between stalk and pore formation (Figure 2G) when hemifusion diaphragms expand (Figures 3F, 4, and 6) during the lipid bilayer fusion reaction to control the extent of fragment formation. Specifically, GTPase activation by GTPγS promotes stalk formation and addition of rVam7 promotes rapid pore formation. The latter finding supports work by many groups studying fusion of synthetic proteoliposomes or vacuolar lysosomes in which mutations that either weaken SNARE bundle interactions (e.g., Vam7-Q283R) or replace transmembrane domains with lipid anchors (Karunakaran and Fratti, 2013; Pieren *et al.*, 2015) stall the reaction immediately before pore formation, causing hemifusion intermediates to accumulate. Similarly, adding bulky protein tags to the lumenal C-termini of SNAREs permits all subreactions up to pore formation, suggesting that tight assembly of lumenal ends of their transmembrane domains drive inner leaflet merger (D'Agostino *et al.*, 2016). Accessory proteins control the rate of SNARE-mediated pore formation during vesicle fusion to coordinate fast neurotransmitter release from synaptic vesicles, for example (Li *et al.*, 2016, Südhof, 2013). However, we speculate that this process is repurposed during lysosome fusion for regulating intralumenal fragment formation that mediates turnover of lipids and proteins.

Consistent with previous work (Reese and Mayer, 2005; Jun and Wickner, 2007), we find that GTPγS promotes stalk formation and alters the transition from hemifusion to pore formation during organelle fusion. Although we did not identify a target, we speculate that GTPγS activates, at least in part, the Rab-GTPase Ypt7 because it is activated by GTPγS in our organelle preparations (Eitzen *et al.*, 2000; Brett *et al.*, 2008) and required for organelle membrane tethering and docking before lipid bilayer merger (Mayer and Wickner, 1997). However, how would Rab activation promote stalk formation? During Ypt7-mediated docking, three events occur that may be enhanced by GTPγS to promote stalk formation: Ca^{2+} efflux (Merz and Wickner, 2004), accumulation of fusogenic lipids at the vertex ring (Fratti *et al.*, 2004), and HOPS recruitment and *trans*-SNARE complex assembly (Seals *et al.*, 2000).

Calcium ions can drive lipid mixing, either directly by forming an anhydrous *trans* complex between phospholipids on apposing membrane outer leaflets of protein-free liposomes (Wilschut *et al.*, 1980) or indirectly by binding C2-domains within synaptotagmin or synaptotagmin-like proteins (Brouwer *et al.*, 2015). Ca^{2+} is released after Ypt7-mediated docking but before pore formation during vacuole fusion (Merz and Wickner, 2004). However, the only synaptotagmin-like proteins in *S. cerevisiae* (called tricalbins; Manford *et al.*, 2012) have not been implicated in this fusion event. Instead calmodulin, a soluble protein unrelated to synaptotagmins, seems to respond to Ca^{2+} and drives downstream mechanisms responsible for pore formation (Peters and Mayer, 1998). Furthermore, GTPγS does not increase Ca^{2+} efflux during homotypic vacuole fusion (unpublished data), which would be needed to enhance lipid mixing if a direct binding mechanism was involved. Thus it seems unlikely that Ca^{2+} mediates enhanced stalk formation by GTPγS through either of these mechanisms.

Membrane lipid content is critical for all subreactions of bilayer fusion before pore formation (Reese and Mayer, 2005; Zick *et al.*, 2014; Lai *et al.*, 2015), and liposomes can undergo lipid mixing, albeit less efficiently, without assistance from proteins (Lee and Lentz, 1997). Thus one possibility is that Ypt7-mediated lipid reorganization at the vertex ring, a region of high membrane curvature, may contribute to stalk formation when organelle membranes are docked within close proximity. Concomitantly, active Ypt7 recruits its cognate effector complex HOPS to this site, which could also contribute to stalk formation through two mechanisms: Vps41, a Ypt7 effector protein within the HOPS complex, contains an amphipathic lipid-packing sensor (ALPS) domain that inserts itself into the outer leaflet of the membrane at the vertex ring (Cabrera *et al.*, 2010). In addition to stabilizing HOPS on membranes (Ho and Stroupe, 2016), it could also deform the outer leaflets in a way that promotes stalk formation. Vps33, an SM protein within HOPS, may also contribute to lipid mixing. Vps33 facilitates *trans* interactions between Nyv1 and Vam3 on apposing membranes (Baker *et al.*, 2015) to promote SNARE-complex assembly before stalk formation (Reese *et al.*, 2005). Vam3, a syntaxin orthologue, is the only vacuolar SNARE whose transmembrane domain seems to play an additional role in stalk formation (Pieren *et al.*, 2015). Thus it is possible that formation of partially zippered *trans*-SNARE complexes may reorient the transmembrane domain of Vam3, bending the outer leaflets at the vertex ring to initiate lipid mixing between apposed membranes. Of

note, the intermembrane distance observed (~8 nm; Figure 6C) would support initial assembly of *trans*-SNARE complexes (Li *et al.*, 2007). In addition to coordinating the transition from stalk to pore formation by SNAREs (Pieren *et al.*, 2010), Vps33 within HOPS proofreads *trans*-SNARE complexes to ensure fusogenicity (Starai *et al.*, 2008). Although speculative, this may explain why pretreating isolated vacuoles with GTPγS suppresses effects of rVam7 on fusion intermediates and outcomes (Figures 2 and 3), by which GTPγS engages Ypt7 and HOPS to enforce SNARE proofreading, which is otherwise bypassed (Thorngren *et al.*, 2004). Thus this proofreading mechanism may account for the delay between stalk and pore formation. In the future, we aim to test the hypothesis that GTPγS targets the Rab-GTPase Ypt7 and its effector complex HOPS and further study their roles in intralumenal fragment formation for controlling lysosomal lipid and protein turnover.

Effect on lysosome physiology

As previously shown, lysosomal polytopic proteins such as Vph1 and Cot1 are present in the contact area between organelles that is internalized into the lumen and degraded upon lysosomal vacuole fusion at the vertex ring (Wang *et al.*, 2002). Here we demonstrate that these membrane proteins can be excluded from this membrane interface and are spared when hemifusion persists during the bilayer fusion reaction (Figure 3). Other nonpolytopic proteins are found in the boundary (e.g., Vac8, a soluble, membrane-associated protein; Wang *et al.*, 2002), but we did not test whether they are also cleared from this area when hemifusion persists. Thus we cannot exclude the possibility that this process also regulates degradation of membrane-associated proteins. Altering the activities of fusion machinery proteins affects hemifusion and determines the extent of membrane internalized during a fusion event. Thus, in addition to affecting size and shape of the fusion product (Figures 1B and 2J), we speculate that targeting the activities of fusion proteins may regulate the turnover of lysosomal membrane proteins in response to osmotic shock (Brett and Merz, 2008), cell division (Weisman, 2006), or aging (Hughes and Gottschling, 2012), for example (Figure 6E). Recently we discovered that lysosomal polytopic proteins are selectively sorted into the boundary for degradation in response to substrate levels, target of rapamycin signaling, or damage caused by heat stress (McNally *et al.*, 2016). Named the intralumenal fragment pathway, this process functions independently of the endosomal sorting complex required for transport machinery responsible for sorting surface polytopic proteins for degradation (Katzmann *et al.*, 2002). Instead, protein sorting requires the docking machinery (Ypt7 and HOPS), suggesting that it may coordinate protein sorting with fragment formation to optimize protein turnover. This machinery is evolutionarily conserved (Nickerson *et al.*, 2009) and responsible for heterotypic lysosome fusion events (e.g., with autophagosomes or late endosomes; Wartosch *et al.*, 2015). Thus we speculate that fragment formation may provide a mechanism to reorganize membrane lipid and protein composition to maintain lysosomal identity during heterotypic fusion events or modify lysosome morphology and function in metazoan cells.

MATERIALS AND METHODS

Yeast strains and reagents

Vacuoles isolated from the *S. cerevisiae* strain BJ3505 (*MATα pep4::HIS3 prb1-Δ1.6R his3-Δ-Tα pep4-801 trp1-Δ101 (gal3) ura3–52 gal2 can1*) were used for vacuole lipid mixing assays and examination by electron microscopy (Haas, 1995; Jun and Wickner, 2007). Vacuole content mixing assays used BJ3505 strains transformed with pYJ406-Fos-ω and pYJ404-Fos-ω or pYJ406-α-Jun and pYJ404-α-Jun (Jun and Wickner, 2007). For total internal reflection fluorescence (TIRF) microscopy, vacuoles were isolated from SEY6210 strains expressing Vph1-GFP (*MATα leu2-3 leu2-112 ura3- 52 his3-Δ-his3u2-3 leu2-11- 801 suc2-Δ9 pep4::HIS3 VPH1-GFP(TRP1)*; Jun and Wickner, 2007) or Cot1-GFP (*MATa his3-Δ1 leu2-Δ0 met15-Δ0 ura3-Δ0 Cot1-GFP::HIS3MX*; Huh *et al.*, 2003). All biochemical and yeast growth reagents were purchased from Sigma-Aldrich, Invitrogen, or BioShop Canada. Proteins used include recombinant Gdi1 purified from bacterial cells using a calmodulin-binding peptide intein fusion system (Brett and Merz, 2008), recombinant Gyp1-46 (the catalytic domain of the Rab-GTPase–activating protein Gyp1), purified as previously described (Eitzen *et al.*, 2000), and recombinant soluble Q_c-SNARE Vam7, purified as previously described (Schwartz and Merz, 2009). Reagents used in fusion reactions were prepared in 10 mM 1,4-piperazinediethanesulfonic acid (PIPES)–sorbitol buffer (PS; PIPES-KOH, pH 6.8, and 200 mM sorbitol).

Vacuole isolation and fusion assays

Vacuoles were isolated from yeast cells as previously described (Haas, 1995). Vacuole lipid mixing assays were conducted using octadecyl rhodamine B (R18) as previously described (Jun and Wickner, 2007), with minor modifications. To obtain R18-labeled vacuoles, 300 µg of vacuoles isolated from BJ3505 cells was incubated with 150 µM R18 for 10 min at 4°C and then reisolated using a Ficoll gradient and ultracentrifugation (105,200 × *g* for 30 min at 4°C). To measure vacuole lipid bilayer mixing, we prepared reactions (180 µl) containing 4 µg of R18-labeled vacuoles and 32 µg of unlabeled vacuoles in standard fusion buffer containing 125 mM KCl, 5 mM $MgCl_2$, ATP-regenerating system (1 mM ATP, 40 mM creatine phosphate, 0.5 mg/ml creatine kinase), and 10 µM CoA in PS buffer. Where indicated, vacuoles were pretreated with GTPγS for 10 min at 27°C before addition to fusion reactions or reactions were supplemented with 100 nM rVam7 and 10 µg/ml bovine serum albumin. Reactions were transferred to black, half-volume, 96-well, flat-bottom microtiter plates, and rhodamine fluorescence (λ_{ex} = 544 nm; λ_{em} = 590 nm) was then measured using a BioTek Synergy H1 plate-reading fluorometer. Readings were taken every 2 min for 50 min at 27°C. Data shown were normalized to values obtained at 50 min under standard fusion conditions. Vacuole content mixing was assessed using a complementary, split β-lactamase–based assay (Jun and Wickner, 2007). In brief, vacuoles were isolated from yeast expressing either CPY50-Jun-GS-α or CPY50-Fos-GS-ω within the vacuole lumen. A 6-µg amount of vacuoles from each strain was added to 60-µl fusion reactions in standard fusion buffer supplemented with 11 µM recombinant glutathione *S*-transferase–Fos protein to reduce background caused by lysis. Reactions were incubated up to 120 min at 27°C and then stopped by placing them on ice. Content mixing was quantified by measuring the rate of nitrocefin hydrolysis by reconstituted β-lactamase. Data shown were normalized to values obtained at 120 min under standard fusion conditions.

Highly inclined and laminated optical sheet microscopy using a TIRF microscope

Live yeast cells stained with FM4-64 to label vacuole membranes were prepared for imaging using a pulse-chase method as previously described (Brett *et al.*, 2008). Fusion reactions (30 µl) were prepared with 6 µg of vacuoles isolated from strains expressing Vph1-GFP or Cot1-GFP in standard fusion reaction buffer with or without 0.2 mM GTPγS or 100 nM rVam7. Before addition to reaction buffer, membranes were stained with FM4-64 by treating vacuoles with 3 µM FM4-64 for 10 min at 27°C. Reactions were incubated for 30 min at 27°C and placed on ice before visualization by highly

inclined and laminated optical sheet (HILO) microscopy to minimize detection of the fluorescence signal above and below the plane of focus (Tokunaga *et al.*, 2008). We used a Nikon Eclipse TiE inverted microscope equipped with a motorized laser TIRF illumination unit, a Photometrics Evolve 512 electron-multiplying charge-coupled device, an ApoTIRF 1.49 numerical aperture/100× objective lens, and bright (50 mW) blue and green solid-state lasers operated with Nikon Elements software (housed in the Center for Microscopy and Cellular Imaging at Concordia University, Montreal, Canada). Cross-sectional images were recorded 1 µm into the sample, and resulting micrographs were deconvolved using AutoQuant X3 (Media Cybernetics) and processed using ImageJ software (National Institutes of Health, Bethesda, MD) and Photoshop CC (Adobe). Images shown were adjusted for brightness and contrast and inverted and sharpened with an unsharp masking filter. Fluorescence intensity profiles of GFP fluorescence were generated using ImageJ software.

Transmission electron microscopy

Isolated vacuoles have been examined by TEM previously (Indge, 1968; Schwencke and De Robichon-Szulmajster, 1976; Wiemken *et al.*, 1979; Horst *et al.*, 1999; Michaillat *et al.*, 2012) but not under conditions that promote fusion. Furthermore, these published micrographs do not clearly resolve lipid bilayers or present abnormal vacuole morphologies, possible artifacts of fixation or processing methods used for imaging. Thus, for our studies, we optimized osmium-based staining, fixation, and Epon embedding methods to preserve vacuole morphology. Fusion reactions were incubated at 27°C for 10 or 30 min, and vacuoles were gently pelleted (5000 × *g* for 5 min) at 4°C and immediately fixed with 2.5% glutaraldehyde in 0.1M cacodylate buffer (pH 7.4) overnight at 4°C. Vacuole pellets were washed with 0.1 M sodium cacodylate (three times, 10 min) and then fixed with 1% osmium tetroxide for 2 h at 4°C. Pellets were washed with water (three times, 5 min), followed by gradual dehydration in ethanol (30–100%) and 100% propylene oxide. Pellets were infiltrated with Epon:propylene oxide for 1 h and then embedded in pure Epon by polymerization (48 h at 57°C). Samples were cut into 100-nm-thick sections using an ultra diamond knife and Reichert Ultracut II microtome, loaded onto 200-mesh copper grids, and stained with uranyl acetate (8 min) and Reynold's lead (5 min). Sections were imaged at 120 kV using an FEI Tecnai 12 TEM outfitted with a Gatan Bioscan digital camera (1k × 1k pixels) housed in the Facility for Electron Microscopy Research (FEMR) at McGill University (Montreal, Canada). For each condition, images were obtained from at least three separate vacuole fusion reactions. Micrographs shown were adjusted for brightness and contrast and sharpened with an unsharp masking filter using Photoshop CC software.

Electron tomography

Epon-embedded vacuole fusion reactions were cut into thick sections (250 nm) for electron tomography and transferred onto carbon-coated copper grids. Images were acquired using an FEI G2 F20 Cryo-STEM outfitted with a Gatan Ultrascan (4k × 4k pixel) digital camera system (FEMR) at a nominal magnification of 9600 times, corresponding to a pixel size of 1.17 nm, using a –60 to 60° tilt. For electron tomography, data collection was done at an electron dose of ~1500 electrons/Å^2 per tomogram. Focusing was done on an adjacent area in order to minimize electron dose exposure. Tilt series were taken using the FEI software in the angular range between –60 and +60° with 2° increments in low tilts (up to 30°) and 1° increments at high tilts (from 31 to 60°). The images were then aligned, cropped, and binned using ETomo IMOD software. The images and movie of the three-dimensional membrane reconstruction by guided segmentation were prepared using Amira Resolve RT 5.2.2 software. Two hemifusion diaphragms were reconstructed.

Cryo–electron microscopy

Aliquots of vacuole fusion reactions (5 µl) were directly blotted (for 5 s) on a charged copper mesh grid using an FEI Vitrobot, rapidly frozen in liquid ethane, and stored in liquid nitrogen until viewed. Frozen samples were imaged using an FEI Tecnai G2 F20 200 kV Cryo-S or FEI Titan Krios 300 kV Cryo-S electron microscope outfitted with Gatan Ultrascan 4000 (4k × 4k pixel) digital camera systems housed in the FEMR. Images were obtained from four separately prepared vacuole fusion reactions. Micrographs shown were adjusted for brightness and contrast using Photoshop CC software.

Data analysis and presentation

For quantitative analysis of electron micrographs, we considered only structures entirely encased by a clearly defined osmium-stained membrane that had distinguishing features indicative of vacuoles, for example, spherical, >400 nm in diameter, and containing lumenal osmium-staining patterns suggestive of lipid deposits or internalized membrane fragments. Average line density plots were generated using ImageJ software. Linear density was plotted every 10 nm perpendicular to docked membranes in the areas indicated in Figure 4E. These data were normalized and aligned based on the maximum density value obtained. Intermembrane distances at docked vacuole interfaces were calculated by measuring the distance between the midpoints of the density peaks representing each membrane. Centroid-to-centroid or manual measurements were also performed; all methods produced similar results. Vacuole surface areas were calculated using the average of two diameter measurements for each vacuole and the assumption that they are spherical. To calculate changes in surface area relative to fusion, we subtracted organelle surface area values measured before fusion (at $t = 0$ min) from surface area values obtained after fusion (at 90 min). These values were then normalized to the number of fusion events by dividing them by content mixing values obtained at 90 min. Boundary lengths of vacuole interfaces were calculated as a percentage of the vacuole circumference (calculated using diameter measurements) represented by the interface between two vacuole membranes (measured as the distance along apposed flattened membranes within 10-nm proximity). We are confident that the intralumenal fragments observed were products of the in vitro membrane fusion reaction because 1) most fusion products imaged were larger than a typical yeast cell (>4 µm in diameter), suggesting they were generated in vitro, 2) we assayed content mixing to confirm that robust fusion occurred before imaging of the reaction (120 min after stimulating fusion), and 3) only 4.8% of isolated vacuoles contained a fragment before initiating fusion ($n = 556$). Unless indicated, data are reported as mean ± SEM and mean. Comparisons were performed using Student's two-tailed *t* tests; $p < 0.05$ indicates significant differences. Quantitative data were plotted using Synergy KaleidaGraph 4.0 software. Figures were prepared using Adobe Illustrator CC software.

ACKNOWLEDGMENTS

We thank K. Basu for technical assistance with electron microscopy. A. J. Merz and M. Sacher provided invaluable discussions and useful feedback. S.M. was supported by a Natural Sciences and Engineering Research Council of Canada Undergraduate Student Research Award and a Fonds de Recherche du Québec Summer Research Scholarship. C.L.B is a Canada Research Chair. This work was supported by Natural Sciences and Engineering Research Council of Canada Grant RGPIN/403537-2011 to C.L.B.

REFERENCES

Baker RW, Jeffrey PD, Zick M, Phillips BP, Wickner WT, Hughson FM (2015). A direct role for the Sec 1/Munc18-family protein Vps33 as a template for SNARE assembly. Science 349, 1111–1114.

Bayer MJ, Reese C, Buhler S, Peters C, Mayer A (2003). Vacuole membrane fusion: V0 functions after trans-SNARE pairing and is coupled to the Ca^{2+}-releasing channel. J Cell Biol 162, 211–222.

Berger AC, Hanson PK, Wylie Nichols J, Corbett AH (2005). A yeast model system for functional analysis of the Niemann-Pick type C protein 1 homolog, Ncr1p. Traffic 6, 907–917.

Brandt T, Cavellini L, Kühlbrandt W, Cohen MM (2016). A mitofusin-dependent docking ring complex triggers mitochondrial fusion in vitro. Elife 5, e14618.

Brett CL, Merz AJ (2008). Osmotic regulation of Rab-mediated organelle docking. Curr Biol 18, 1072–1077.

Brett CL, Plemel RL, Lobinger BT, Vignali M, Fields S, Merz AJ (2008). Efficient termination of vacuole Rab GTPase signaling requires coordinated action by a GAP and a protein kinase. J Cell Biol 182, 1141–1151.

Brouwer I, Giniatullina A, Laurens N, van Weering JR, Bald D, Wuite GJ, Groffen AJ (2015). Direct quantitative detection of Doc2b-induced hemifusion in optically trapped membranes. Nat Commun 6, 8387.

Cabrera M, Langemeyer L, Mari M, Rethmeier R, Orban I, Perz A, Brücker C, Griffith J, Klose D, Steinhoff HJ, *et al*. (2010). Phosphorylation of a membrane curvature-sensing motif switches function of the HOPS subunit Vps41 in membrane tethering. J Cell Biol 191, 845–859.

Chan YH, Marshall WF (2010). Scaling properties of cell and organelle size. Organogenesis 6, 88–96.

Chernomordik LV, Kozlov MM (2008). Mechanics of membrane fusion. Nat Struct Mol Biol 15, 675–683.

Conklin DS, McMaster JA, Culbertson MR, Kung C (1992). COT1, a gene involved in cobalt accumulation in *Saccharomyces cerevisiae*. Mol Cell Biol 12, 3678–3688.

D'Agostino M, Risselada HJ, Mayer A (2016). Steric hindrance of SNARE transmembrane domain organization impairs the hemifusion-to-fusion transition. EMBO Rep 17, 1590–1608.

de Duve C, Wattiaux R (1966). Functions of lysosomes. Annu Rev Physiol 28, 435–492.

Diao J, Grob P, Cipriano DJ, Kyoung M, Zhang Y, Shah S, Nguyen A, Padolina M, Srivastava A, Vrljic M, *et al*. (2012). Synaptic proteins promote calcium-triggered fast transition from point contact to full fusion. Elife 1, e00109.

Diao J, Liu R, Rong Y, Zhao M, Zhang J, Lai Y, Zhou Q, Wilz LM, Li J, Vivona S, *et al*. (2015). ATG14 promotes membrane tethering and fusion of autophagosomes to endolysosomes. Nature 520, 563–566.

Eitzen G, Will E, Gallwitz D, Haas A, Wickner W (2000). Sequential action of two GTPases to promote vacuole docking and fusion. EMBO J 19, 6713–6720.

Floyd DL, Ragains JR, Skehel JJ, Harrison SC, van Oijen AM (2008). Single-particle kinetics of influenza virus membrane fusion. Proc Natl Acad Sci USA 105, 15382–15387.

Forgac M (2007). Vacuolar ATPases: rotary proton pumps in physiology and pathophysiology. Nat Rev Mol Cell Biol 8, 917–929.

Fratti RA, Jun Y, Merz AJ, Margolis N, Wickner W (2004). Interdependent assembly of specific regulatory lipids and membrane fusion proteins into the vertex ring domain of docked vacuoles. J Cell Biol 167, 1087–1098.

Haas A (1995). A quantitative assay to measure homotypic vacuole fusion. Methods Cell Sci 17, 283–294.

Harrison SC (2008). Viral membrane fusion. Nat Struct Mol Biol 15, 690–698.

Hernandez JM, Stein A, Behrmann E, Riedel D, Cypionka A, Farsi Z, Walla PJ, Raunser S, Jahn R (2012). Membrane fusion intermediates via directional and full assembly of the SNARE complex. Science 336, 1581–1584.

Hickey CM, Wickner W (2010). HOPS initiates vacuole docking by tethering membranes before trans-SNARE complex assembly. Mol Biol Cell 21, 2297–2305.

Ho R, Stroupe C (2016). The HOPS/class C Vps complex tethers high-curvature membranes via a direct protein-membrane interaction. Traffic 17, 1078–1090.

Horst M, Knecht EC, Schu PV (1999). Import into and degradation of cytosolic proteins by isolated yeast vacuoles. Mol Biol Cell 10, 2879–2889.

Hughes AL, Gottschling DE (2012). An early age increase in vacuolar pH limits mitochondrial function and lifespan in yeast. Nature 492, 261–265.

Huh W-K, Falvo JV, Gerke LC, Carroll AS, Howson RW, Weissman JS, O'Shea EK (2003). Global analysis of protein localization in budding yeast. Nature 425, 686–691.

Indge KJ (1968). The isolation and properties of the yeast cell vacuole. J Gen Microbiol 51, 441–446.

Jun Y, Wickner W (2007). Assays of vacuole fusion resolve the stages of docking, lipid mixing, and content mixing. Proc Natl Acad Sci USA 104, 13010–13015.

Karunakaran S, Fratti RA (2013). The lipid composition and physical properties of the yeast vacuole affect the hemifusion-fusion transition. Traffic 14, 650–662.

Katzmann DJ, Odorizzi G, Emr SD (2002). Receptor downregulation and multivesicular-body sorting. Nat Rev Mol Cell Biol 3, 893–905.

Knapp PE, Swanson JA (1990). Plasticity of the tubular lysosomal compartment in macrophages. J Cell Sci 95, 433–439.

Lai Y, Zhao L, Bu B, Lou X, Li D, Ji B, Liu J, Diao J, Shin YK (2015). Lipid molecules influence early stages of yeast SNARE-mediated membrane fusion. Phys Biol 12, 025003.

Lee J, Lentz BR (1997). Evolution of lipidic structures during model membrane fusion and the relation of this process to cell membrane fusion. Biochemistry 36, 6251–6259.

Li F, Pincet F, Perez E, Eng WS, Melia TJ, Rothman JE, Tareste D (2007). Energetics and dynamics of SNAREpin folding across lipid bilayers. Nat Struct Mol Biol 14, 890–896.

Li F, Tiwari N, Rothman JE, Pincet F (2016). Kinetic barriers to SNAREpin assembly in the regulation of membrane docking/priming and fusion. Proc Natl Acad Sci USA 113, 10536–10541.

Li J, Deffieu MS, Lee PL, Saha P, Pfeffer SR (2015). Glycosylation inhibition reduces cholesterol accumulation in NPC1 protein-deficient cells. Proc Natl Acad Sci USA 112, 14876–14881.

Luzio JP, Pryor PR, Bright NA (2007). Lysosomes: fusion and function. Nat Rev Mol Cell Biol 8, 622–632.

Manford AG, Stefan CJ, Yuan HL, Macgurn JA, Emr SD (2012). ER-to-plasma membrane tethering proteins regulate cell signaling and ER morphology. Dev Cell 23, 1129–1140.

Mayer A, Wickner W (1997). Docking of yeast vacuoles is catalyzed by the Ras-like GTPase Ypt7p after symmetric priming by Sec 18p (NSF). J Cell Biol 136, 307–317.

McNally EK, Karim MA, Brett CL (2016). Selective lysosomal transporter degradation by organelle membrane fusion. Dev Cell, doi: 10.1016/j.devcel.2016.11.024.

Merz AJ, Wickner WT (2004). Trans-SNARE interactions elicit Ca^{2+} efflux from the yeast vacuole lumen. J Cell Biol 164, 195–206.

Michaillat L, Baars TL, Mayer A (2012). Cell-free reconstitution of vacuole membrane fragmentation reveals regulation of vacuole size and number by TORC1. Mol Biol Cell 23, 881–895.

Mrakovic A, Kay JG, Furuya W, Brumell JH, Botelho RJ (2012). Rab7 and Arl8 GTPases are necessary for lysosome tubulation in macrophages. Traffic 13, 1667–1679.

Nickerson DP, Brett CL, Merz AJ (2009). Vps-C complexes: gatekeepers of endolysosomal traffic. Curr Opin Cell Biol 21, 543–551.

Nikolaus J, Stöckl M, Langosch D, Volkmer R, Herrmann A (2010). Direct visualization of large and protein-free hemifusion diaphragms. Biophys J 98, 1192–1199.

Peters C, Mayer A (1998). $Ca^{2+/c}$almodulin signals the completion of docking and triggers a late step of vacuole fusion. Nature 396, 575–580.

Pieren M, Desfougeres Y, Michaillat L, Schmidt A, Mayer A (2015). Vacuolar SNARE protein transmembrane domains serve as nonspecific membrane anchors with unequal roles in lipid mixing. J Biol Chem 290, 12821–12832.

Pieren M, Schmidt A, Mayer A (2010). The SM protein Vps33 and the t-SNARE H(abc) domain promote fusion pore opening. Nat Struct Mol Biol 17, 710–717.

Pisoni RL, Thoene JG (1991). The transport systems of mammalian lysosomes. Biochim Biophys Acta 1071, 351–373.

Reese C, Heise F, Mayer A (2005). Trans-SNARE pairing can precede a hemifusion intermediate in intracellular membrane fusion. Nature 436, 410–414.

Reese C, Mayer A (2005). Transition from hemifusion to pore opening is rate limiting for vacuole membrane fusion. J Cell Biol 171, 981–990.

Risselada HJ, Bubnis G, Grubmüller H (2014). Expansion of the fusion stalk and its implication for biological membrane fusion. Proc Natl Acad Sci USA 111, 11043–11048.

Schwartz ML, Merz AJ (2009). Capture and release of partially zipped trans-SNARE complexes on intact organelles. J Cell Biol 185, 535–549.

Schwencke J, De Robichon-Szulmajster H (1976). The transport of S-adenosyl-L-methionine in isolated yeast vacuoles and spheroplasts. Eur J Biochem 65, 49–60.

Seals DF, Eitzen G, Margolis N, Wickner WT, Price A (2000). A Ypt/Rab effector complex containing the Sec 1 homolog Vps33p is required for homotypic vacuole fusion. Proc Natl Acad Sci USA 97, 9402–9407.
Starai VJ, Hickey CM, Wickner W (2008). HOPS proofreads the trans-SNARE complex for yeast vacuole fusion. Mol Biol Cell 19, 2500–2508.
Südhof TC (2013). Neurotransmitter release: the last millisecond in the life of a synaptic vesicle. Neuron 80, 675–690.
Thorngren N, Collins KM, Fratti RA, Wickner W, Merz AJ (2004). A soluble SNARE drives rapid docking, bypassing ATP and Sec 17/18p for vacuole fusion. EMBO J 23, 2765–2776.
Tokunaga M, Imamoto N, Sakata-Sogawa K (2008). Highly inclined thin illumination enables clear single-molecule imaging in cells. Nat Methods 5, 159–161.
Veit M, Laage R, Dietrich L, Wang Lnn C (2001). Vac8p release from the SNARE complex and its palmitoylation are coupled and essential for vacuole fusion. EMBO J 20, 3145–3155.
Wang L, Merz AJ, Collins KM, Wickner W (2003). Hierarchy of protein assembly at the vertex ring domain for yeast vacuole docking and fusion. J Cell Biol 160, 365–374.
Wang L, Seeley ES, Wickner W, Merz AJ (2002). Vacuole fusion at a ring of vertex docking sites leaves membrane fragments within the organelle. Cell 108, 357–369.
Warner JM, O'Shaughnessy B (2012). Evolution of the hemifused intermediate on the pathway to membrane fusion. Biophys J 103, 689–701.
Wartosch L, Günesdogan U, Graham SC, Luzio JP (2015). Recruitment of VPS33A to HOPS by VPS16 is required for lysosome fusion with endosomes and autophagosomes. Traffic 16, 727–742.
Weisman LS (2006). Organelles on the move: insights from yeast vacuole inheritance. Nat Rev Mol Cell Biol 7, 243–252.
Wickner W (2010). Membrane fusion: five lipids, four SNAREs, three chaperones, two nucleotides, and a Rab, all dancing in a ring on yeast vacuoles. Annu Rev Cell Dev Biol 26, 115–136.
Wiemken A, Schellenberg M, Urech K (1979). Vacuoles: the sole compartments of digestive enzymes in yeast (*Saccharomyces cerevisiae*)? Arch Microbiol 123, 23–35.
Wilschut J, Düzgünes N, Fraley R, Papahadjopoulos D (1980). Studies on the mechanism of membrane fusion: kinetics of calcium ion induced fusion of phosphatidylserine vesicles followed by a new assay for mixing of aqueous vesicle contents. Biochemistry 19, 6011–6021.
Wu Y, Takar M, Cuentas-Condori AA, Graham TR (2016). Neo1 and phosphatidylethanolamine contribute to vacuole membrane fusion in *Saccharomyces cerevisiae*. Cell Logist 6, e1228791.
Zick M, Stroupe C, Orr A, Douville D, Wickner WT (2014). Membranes linked by trans-SNARE complexes require lipids prone to nonbilayer structure for progression to fusion. Elife 3, e01879.
Zick M, Wickner W (2013). The tethering complex HOPS catalyzes assembly of the soluble SNARE Vam7 into fusogenic trans-SNARE complexes. Mol Biol Cell 24, 3746–3753.